Every organism contains, within its regulatory system, self-sustaining pacemaker circuitry that coordinates progression of the cell cycle. At a high level, all these cell-cycle control circuits exhibit parallels in mechanism and function. For example, phosphorylation pathways are interconnected with transcriptional regulatory networks, critical positive and negative feedback pathways, and targeted proteolysis. These mechanisms lead to the cyclical presence and/or activation state of key regulatory proteins that in turn control the modular functions that implement the cell cycle. The specific cell-cycle regulatory proteins in bacteria and eukaryotic cells are not homologous; rather, the homologies are at the level of system design.

References and Notes

1. M. T. Laub, H. H. McAdams, T. Feldblyum, C. M. Fraser, L. Shapiro, *Science* **290**, 2144 (2000).
2. K. R. Ryan, L. Shapiro, *Annu. Rev. Biochem.* **72**, 367 (2003).
3. H. H. McAdams, L. Shapiro, *Science* **301**, 1874 (2003).
4. U. Jenal, C. Stephens, *Curr. Opin. Microbiol.* **5**, 558 (2002).
5. R. B. Jensen, S. C. Wang, L. Shapiro, *Nature Rev. Mol. Cell Biol.* **3**, 167 (2002).
6. M. T. Laub, S. L. Chen, L. Shapiro, H. H. McAdams, *Proc. Natl. Acad. Sci. U.S.A.* **99**, 4632 (2002).
7. K. C. Quon, G. T. Marczynski, L. Shapiro, *Cell* **84**, 83 (1996).
8. K. C. Quon, B. Yang, I. J. Domian, L. Shapiro, G. T. Marczynski, *Proc. Natl. Acad. Sci. U.S.A.* **95**, 120 (1998).
9. U. Jenal, T. Fuchs, *EMBO J.* **17**, 5658 (1998).
10. A. Reisenauer, L. Shapiro, *EMBO J.* **21**, 4969 (2002).
11. C. Jacobs, I. J. Domian, J. R. Maddock, L. Shapiro, *Cell* **97**, 111 (1999).
12. C. Jacobs, N. Ausmees, S. J. Cordwell, L. Shapiro, M. T. Laub, *Mol. Microbiol.* **47**, 1279 (2003).
13. I. J. Domian, A. Reisenauer, L. Shapiro, *Proc. Natl. Acad. Sci. U.S.A.* **96**, 6648 (1999).
14. E. M. Judd, K. R. Ryan, W. E. Moerner, L. Shapiro, H. H. McAdams, *Proc. Natl. Acad. Sci. U.S.A.* **100**, 8235 (2003).
15. Materials and methods are available as supporting material on *Science* Online.
16. A. C. Meisenzahl, L. Shapiro, U. Jenal, *J. Bacteriol.* **179**, 592 (1997).
17. P. Prentki, H. M. Krisch, *Gene* **29**, 303 (1984).
18. I. J. Domian, K. C. Quon, L. Shapiro, *Cell* **90**, 415 (1997).
19. D. C. Lin, A. D. Grossman, *Cell* **92**, 675 (1998).
20. Microarray data analysis methodology is available as supporting material on *Science* Online.
21. The *Caulobacter* oligo microarray design and methods are described online at www.stanford.edu/group/caulobacter/oligoArrays.
22. D. Y. Hung, L. Shapiro, *Proc. Natl. Acad. Sci. U.S.A.* **99**, 13160 (2002).
23. W. C. Nierman *et al.*, *Proc. Natl. Acad. Sci. U.S.A.* **98**, 4136 (2001).
24. J. M. Sommer, A. Newton, *J. Bacteriol.* **171**, 392 (1989).
25. S. P. Wang, P. L. Sharma, P. V. Schoenlein, B. Ely, *Proc. Natl. Acad. Sci. U.S.A.* **90**, 630 (1993).
26. G. B. Hecht, T. Lane, N. Ohta, J. M. Sommer, A. Newton, *EMBO J.* **14**, 3915 (1995).
27. M. V. Marques, S. L. Gomes, J. W. Gober, *J. Bacteriol.* **179**, 5502 (1997).
28. P. H. Viollier, N. Sternheim, L. Shapiro, *Proc. Natl. Acad. Sci. U.S.A.* **99**, 13831 (2002).
29. R. B. Jensen, L. Shapiro, *Trends Cell Biol.* **10**, 483 (2000).
30. W. B. Crymes, Jr., D. Zhang, B. Ely, *J. Bacteriol.* **181**, 3967 (1999).

31. This study was partly supported by NIH grants GM32506 and GM1426 (L.S.), Department of Energy grant DE-FG03-01ER63219 (H.H.M. and L.S.), Defense Advanced Research Projects Agency grant MDA972-00-1-0032 (H.H.M.), and Office of Naval Research grant N00014-02-1-0538 (H.H.M.). P.B. is supported by a Texas Instruments Stanford Graduate Fellowship.

Supporting Online Material

www.sciencemag.org/cgi/content/full/1095191/DC1
Materials and Methods
SOM Text
Tables S1 and S2
References and Notes

30 December 2003; accepted 26 March 2004
Published online 15 April 2004;
10.1126/science.1095191
Include this information when citing this paper.

REPORTS

Continuous Particle Separation Through Deterministic Lateral Displacement

Lotien Richard Huang,[1] Edward C. Cox,[2] Robert H. Austin,[3] James C. Sturm[1]

We report on a microfluidic particle-separation device that makes use of the asymmetric bifurcation of laminar flow around obstacles. A particle chooses its path deterministically on the basis of its size. All particles of a given size follow equivalent migration paths, leading to high resolution. The microspheres of 0.8, 0.9, and 1.0 micrometers that were used to characterize the device were sorted in 40 seconds with a resolution of ~10 nanometers, which was better than the time and resolution of conventional flow techniques. Bacterial artificial chromosomes could be separated in 10 minutes with a resolution of ~12%.

Particles in solution are usually separated according to size by exclusion or hydrodynamic chromatography (*1*–*5*). In the former, a sample mixture is injected at one end of a tube packed with porous beads and then washed through the tube (*1*–*3*). Particles smaller than the pore size enter the beads, which lengthens their migration path, and so they are on average eluted later than larger particles. Zones of particles of a given size broaden, however, because particles in each zone take many different paths, leading to different retention times. This multipath effect reduces the resolution of size-exclusion chromatography (*6*–*8*). In hydrodynamic chromatography, a sample mixture is driven through a capillary by hydrodynamic flow, which has a parabolic flow profile (*4*, *5*). Large particles cannot intercept the low-velocity fluid near the capillary wall, and thus on average move faster and become separated from small particles. Multipath effects also limit the resolution of hydrodynamic chromatography, because each migration path samples different velocities in the parabolic flow (*9*, *10*).

Recently, devices that exploit both techniques have been miniaturized with the use of microfabrication technology (*5*, *10*–*12*). Microfabricated devices have also been designed that inherently rely on diffusion for separation. Particle mixtures are either repeatedly subject to spatially asymmetric potentials created by microelectrodes (*13*) or driven through arrays of micrometer-scale asymmetric obstacles (*14*–*16*) to exploit differences in diffusion lengths. In all of the devices discussed so far, particles in a given zone have many different migration paths, and diffusion is required for separation.

Here, we demonstrate a separation process that creates equivalent migration paths for each particle in a mixture, thereby eliminating multipath zone broadening (Fig. 1). The separation process uses laminar flow (*17*, *18*) through a periodic array of micrometer-scale obstacles. Each row of obstacles is shifted horizontally with respect to the previous row by $\Delta\lambda$, where λ is the center-to-center distance between the obstacles (Fig. 1A). For convenience, let $\Delta\lambda/\lambda$ be 1/3. Fluid emerging from a gap between two obstacles will encounter an obstacle in the next row and will bifurcate as it moves around the obstacle. Let the flow diverted to the left of the obstacle be $\delta\Phi$, where Φ is the total fluid flux

[1]Department of Electrical Engineering, [2]Department of Molecular Biology, [3]Department of Physics, Princeton Institute for the Science and Technology of Materials (PRISM), Princeton University, Princeton, NJ 08544, USA.

going through the gap. If the fluid is confined to move straight down through the array, δ must be equal to Δλ/λ. Let us then consider the flow through a gap to be made up of three lanes, each of which by definition has a flux of Φ/3. Because the Reynolds number is low ($\approx 10^{-3}$ in micrometer-scale environments) and flows are laminar, the streams in each lane do not cross or mix (*17*, *18*) (Fig. 1B). Notably, as the lanes go through gaps, their positions relative to the gaps change. We represent the lanes in each gap by 1, 2, and 3, from left to right, respectively. Lane 1 becomes lane 3 in the next gap, lane 2 becomes lane 1, and lane 3 becomes lane 2 (Fig. 1B). After three rows, the three lanes rejoin in their original configuration.

Particles that are smaller than the lane width will follow the streamlines (*18*). A particle starting in lane 1 will go through lane 3 (right lane with respect to the gap) in the second row, lane 2 (middle lane) in the third row, and back to lane 1 (left lane) in the fourth row (Fig. 1B). In fact, particles starting from any of the three lanes will go back to the original lane assignment after three rows, so that net migration is in the average flow direction. We call this motion the "zigzag mode." In practice, particles can diffuse into an adjacent lane. However, the microscopic path for all lanes is equivalent, unlike the multiple paths particles take when moving through a column of porous beads.

In contrast to the smaller particles, a particle with a radius larger than the width of lane 1 at a gap will behave differently in the array. This is because the center of the particle cannot "fit" into lane 1 in a gap. As such a particle from lane 2 in one gap moves into the subsequent gap, expecting to move through the gap in lane 1, the particle will be "bumped" and its center will thus be displaced into lane 2 (Fig. 1C). The particle will then flow with the fluid in lane 2. This process is repeated every time a large particle approaches a row of obstacles, so that the particle remains in lane 2 as it moves down through the array. We call this transport pattern the "displacement mode." This theory is also applicable to electrophoresis by considering ion flows instead of fluid flows.

To test these ideas, we microfabricated a device in silicon consisting of a matrix of obstacles as in Fig. 1, in which the horizontal obstacle spacing λ was 8 μm, the row-to-row spacing was 8 μm, and the gap width $d = 1.6$ μm (fig. S1). Each row was shifted laterally by 0.1λ, providing 10 lanes, rather than the three discussed above. Particles were injected from a 10-μm-wide channel at the top of the matrix and were carried across the matrix by fluid flow.

The two transport modes, zigzag and displacement, were experimentally observed with the use of fluorescent polystyrene microspheres (Duke Scientific Corporation, Palo Alto, CA) with diameters of 0.40 and 1.03 μm in aqueous buffer (Fig. 2A) (*19*) and imaged by fluorescence microscopy with a long exposure time to reveal single-particle trajectories. The varying brightness along each trajectory reflects the different flow speeds of a bead in the matrix; the trajectory in the narrow gaps appears dimmer because of the higher flow speed and shorter residence time. The 0.40-μm bead (green) stayed in one lane, crossing a column of obstacles approximately every 10 rows (zigzag mode). In contrast, the 1.03-μm bead (red) was displaced by the obstacles in every row (displacement mode). The device did not clog or jam because the gap size is larger than the particles being separated.

To probe the transition between the two transport modes, fluorescent beads with diameters of 0.60, 0.70, 0.80, 0.90, and 1.03 μm were mixed and injected into the matrix (*20*). The beads were separated into different streams at a flow speed of ~40 μm/s, created by a driving pressure of 3 kPa. The fluorescence profile 11 mm from the injection point is shown in Fig. 2B. The measured migration directions with respect to the flow, defined as the migration angles, are plotted as a function of the bead diameter in Fig. 2C, which shows that at 40 μm/s the transition from the zigzag to the displacement mode is gradual. The smooth transition is probably due to Brownian motion of the particles between lanes. At a flow speed of 40 μm/s, a 0.6-μm particle has a diffusion length of ~0.54 μm over the 0.2 s it takes to move the 8 μm from one gap to the next (*21*). This is a factor of 3 larger than the average lane width at a gap, which is about 0.16 μm (there are 10 lanes in a gap of 1.6 μm). Thus, it is not surprising that we observe a gradual rather than an abrupt change from zigzag mode to displacement mode as the particle size is increased.

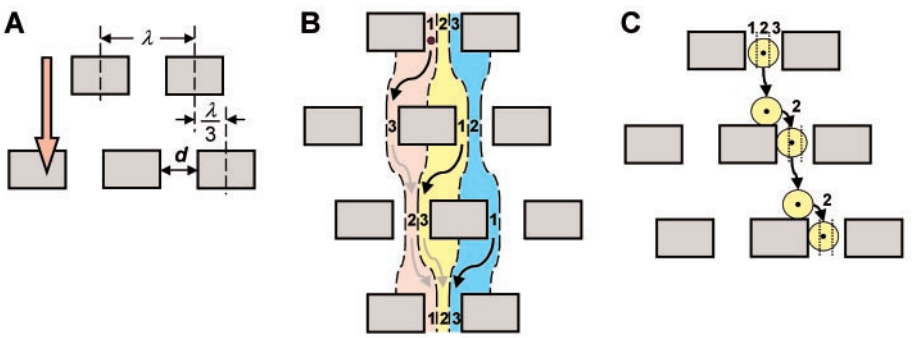

Fig. 1. (**A**) Geometric parameters defining the obstacle matrix. A fluid flow is applied in the vertical direction (orange arrow). (**B**) Three fluid streams (red, yellow, and blue) in a gap do not mix as they flow through the matrix. Lane 1 at the first obstacle row becomes lane 3 at the second row, lane 3 becomes lane 2 at the third row, and so on. Small particles following streamlines will thus stay in the same lane. (**C**) A particle with a radius that is larger than lane 1 follows a streamline passing through the particle's center (black dot), moving toward lane 1. The particle is physically displaced as it enters the next gap. Black dotted lines mark the lanes.

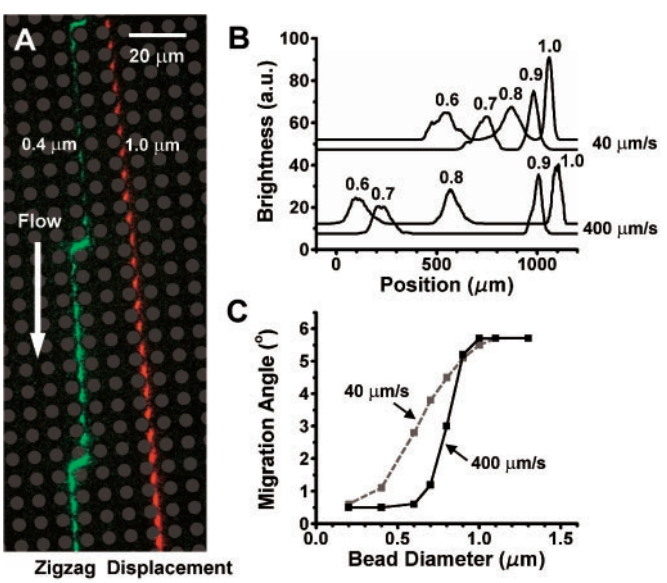

Fig. 2. (**A**) Fluorescent images of microspheres migrating in the matrix, showing trajectories of the two transport modes. The flow speed is ~400 μm/s, created by a pressure of 30 kPa. The gray dots, which represent the obstacles, are superimposed on the fluorescent image. (**B**) Fluorescence profiles of microspheres separated with flow speeds of ~40 μm/s (upper curves) and ~400 μm/s (lower curves) scanned at ~11 mm from the injection point. The beads with diameters of 0.60, 0.80, and 1.03 μm are green fluorescent, whereas those with diameters of 0.70 and 0.90 μm are red, and thus each scan is shown as two curves representing the two colors. a.u., arbitrary units. (**C**) Measured migration angles as a function of microsphere diameter at two different flow speeds.

To minimize diffusion effects, the flow velocity was raised by a factor of 10 to ~400 μm/s, which reduced the running time to ~40 s. A much sharper transition occurred (Fig. 2C). The transition between the two modes occurred at a particle size of ~0.8 μm. This can be modeled as follows: Assume that the flow has a parabolic profile at each gap, with flow velocity pinned to zero at the obstacle walls. Because 10% of the fluid flux occupies ~20% of the gap width d (1.6 μm), the critical diameter is $2 \times 20\% \times d$, or 0.64 μm. This agrees reasonably well with the experimental data.

Rather than sorting based on a single critical particle size, the matrix can have varying gap widths to resolve a spectrum of particle sizes. We fabricated a device containing nine sections, each of which had a different gap width, ranging from 1.4 to 2.2 μm in increments of 0.1 μm (Fig. 3). The varying gap widths were designed to tune the critical diameter in nine steps from ~0.70 to ~1.10 μm, so that a given sized particle would switch transport mode as it ran through the matrix.

Beads of diameters 0.80, 0.90, and 1.03 μm were injected into this matrix with stepped gaps (Fig. 3) and set to flow at ~400 μm/s. At the top of the matrix, the gaps have a critical size smaller than the beads so that all particles follow the displacement mode. The 0.80-μm beads (green) quickly switched to the zigzag mode as the gap size increased. The 0.90-μm beads changed their flow behavior in the fourth section, and the 1.03-μm microspheres made the transition at the eighth section. The fluorescence intensity profile scanned ~14 mm from the injection point showed that the peaks of 0.80, 0.90, and 1.03 μm had coefficients of variation (CVs) of 1.1, 1.2, and 1.9%, respectively (red error bars in Fig. 3, centered at the means of the peaks) (*22*). In comparison, the 1% CV attributable to inhomogeneity of the bead population, measured by the manufacturer with quasi-elastic laser light scattering and transmission electron microscopy, is shown as the black error bars underneath the peaks. Thus, the size uncertainty introduced by the physics of our device is at worst 1 to 2% of the particle size, or less than 20 nm. This resolution may be compared favorably to hydrodynamic chromatography and quasi-elastic laser light scattering, which can resolve particles in this size range to an accuracy of 15 and 3%, respectively (*5*, *23*). Electron microscopy can resolve particle sizes to <1% (*24*), but it requires off-line measurement of the particles and is not practical for sorting.

The crucial difference between this device and the sorting methods mentioned earlier is that it fundamentally does not depend on diffusion or multipath averaging. For example, in one set of earlier work, particles were separated because some diffuse far enough to be "ratcheted" by asymmetric microfabricated obstacles (*13*–*16*). Diffusion was critical for the device operation; separation worked better at low flow speeds than at high speeds. In the device presented here, the separation of the particles is based on a deterministic event (the physical displacement), not on a random process. Some random diffusion of particles in our device across streamlines is inevitable, but it only moderately degrades the resolution because the paths to which particles could move by diffusion are essentially equivalent to their original ones. Furthermore, such diffusion effects can be minimized by high flow speeds (Fig. 2C).

Our technique can separate flexible biological molecules without jamming or clogging. In particular, we prepared bacterial artificial chromosomes, a widely used DNA source for many genomics projects (*25*), from *Escherichia coli* by means of standard protocols (*25*–*27*). These molecules tend to coil up and can thus be approximated as soft spheres. Electric fields were used to drive the molecules through the matrix (*27*). These fields created electric currents, which were bifurcated in the matrix in the same manner as fluid flow in the earlier example with beads. Bacterial artificial chromo-

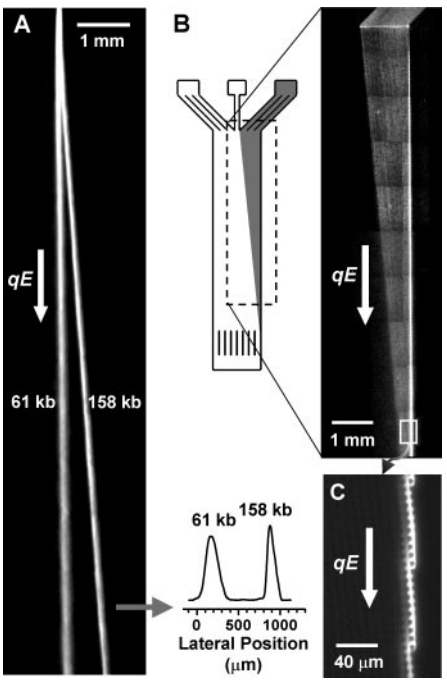

Fig. 4. (**A**) Fluorescence micrograph showing separation of bacterial artificial chromosomes and the electrophoretogram scanned at 12 mm from the injection point. The device was made in fused silica with a constant gap width of d = 3 μm, λ = 8 μm, and 10% shift. Bacterial artificial chromosome DNAs (61 and 158 kb at 2 and 1 μg/ml, respectively) were electrophoresed through the device with a field of ~12 V/cm. Bands were identified by observing the molecules' sizes with a 60X objective. qE represents the electric force (of charge q and field E) exerted on DNA. (**B**) Schematic diagram and fluorescence micrograph showing the device as a DNA concentrator, with a field of ~10 V/cm. DNA was loaded in the top-right reservoir (fig. S1) and injected from the top edge of the matrix by an electric field in a device with constant gaps of d = 1.5 μm. Because of the small gaps, both species of DNA moved in displacement mode toward the right edge of the matrix and accumulated against that edge. (**C**) High-magnification fluorescence micrograph showing DNA molecules accumulating against an edge of the matrix. The fluorescence intensity at the edge increased linearly with the distance from the top, indicating the continuous enrichment of the DNA. At 12 mm from the top, the intensity increased by a factor of 150.

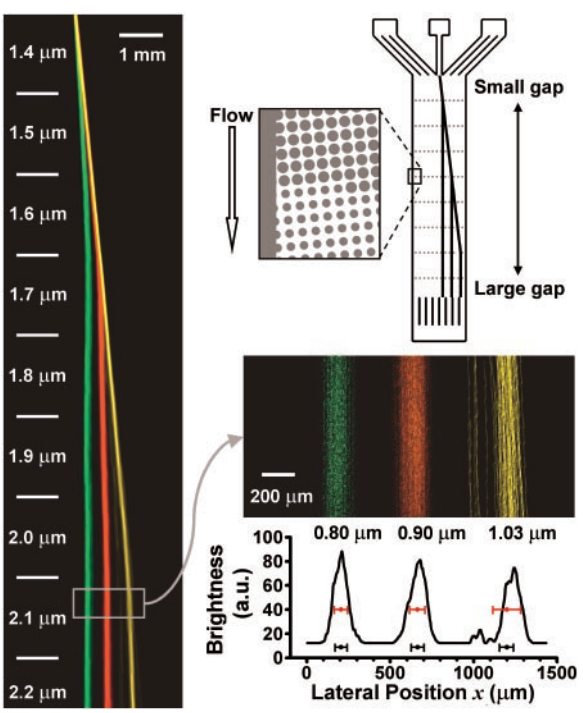

Fig. 3. High-resolution separation of fluorescent microspheres with diameters of 0.80 μm (green), 0.90 μm (red), and 1.03 μm (yellow), with a matrix of varying gap size. Whereas the shift in registry and the lattice constants of the matrix remain the same, the obstacle diameters are changed to create gaps, d, of different sizes, which are labeled on the left side of the fluorescent image. The red bars on the fluorescence profile represent the width of the peaks (±SD), and the black bars label the ±1% inhomogeneity in the bead population. a.u., arbitrary units.

somes of 61 and 158 kb were separated into two bands, with widths that corresponded to CVs of ~12 and ~5% (molecular weight), respectively (Fig. 4) (*28*), in a field of ~12 V/cm, creating a migration speed of ~20 μm/s. Higher fields result in reduced separation, possibly because of random deformation and stretching of DNA, which are caused by collisions with obstacles. Even so, the running time for this experiment was only 10 min, comparable to other nonconventional techniques for separation of DNA larger than ~40 kb (*29*). In contrast, the standard method for separating large DNA typically requires many hours for the same resolution (*25*, *26*).

The DNA separation work presented here differs fundamentally from our earlier work in microfabricated arrays. In one set of that work (*15*, *16*), the separation inherently relies on diffusion. In a second approach, alternating electric fields in different directions were used to elongate DNA in a hexagonal post array (*30*). The method used here is a dc method without pulsing and does not rely on "linear" molecules.

In summary, we have demonstrated a new technique for continuous particle separation according to size, which has better resolution than conventional techniques. We believe that as the gap size is reduced using nanofabrication, this device can be used to fractionate and perhaps even identify biological supramacromolecules, such as viral particles and protein complexes.

References and Notes

1. E. Heftmann, *Chromatography: Fundamentals and Applications of Chromatographic and Electrophoretic Methods* (Elsevier Science, New York, ed. 4, 1983).
2. J. C. Giddings, *Nature* **184**, 357 (1959).
3. L. Dupont, G. J. Mortha, *J. Chromatogr. A* **1026**, 129 (2004).
4. E. A. DiMarzio, C. M. Guttman, *Macromolecules* **3**, 131 (1970).
5. M. T. Blom *et al*., *Anal. Chem.* **75**, 6761 (2003).
6. T. K. Perkins, O. C. Johnston, *Soc. Pet. Eng. J.* **3**, 70 (1963).
7. G. I. Taylor, *Proc. R. Soc. London Ser. A* **219**, 186 (1953).
8. R. Aris, *Proc. R. Soc. London Ser. A* **235**, 67 (1956).
9. J. C. Giddings, *Science* **260**, 1456 (1993).
10. J. Janca, J. F. Berneron, R. Boutin, *J. Colloid Interface Sci.* **260**, 317 (2003).
11. M. Baba *et al*., *Appl. Phys. Lett.* **83**, 1468 (2003).
12. T. Sano *et al*., *Appl. Phys. Lett.* **83**, 4438 (2003).
13. J. Rousselet, L. Salome, A. Ajdari, J. Prost, *Nature* **370**, 446 (1994).
14. S. G. van Oudenaarden, S. G. Boxer, *Science* **285**, 1046 (1999).
15. F. Chou *et al*., *Proc. Natl. Acad. Sci. U.S.A.* **96**, 13762 (1999).
16. L. R. Huang *et al*., *Anal. Chem.* **75**, 6963 (2003).
17. R. P. Feynman, R. B. Leighton, M. Sands, *The Feynman Lectures on Physics* (Addison-Wesley, Reading, MA, 1966), vol. 2, chap. 41.
18. J. Happel, H. Brenner, *Low Reynolds Number Hydrodynamics: With Special Applications to Particulate Media* (Sijthoff & Noordhoff, Leiden, Netherlands, ed. 2, 1973).
19. A 0.1x Tris-Borate-EDTA (TBE) buffer containing 0.02% performance-optimized linear polyacrylamide (POP)–6 (Perkin-Elmer Biosystems) was used in the experiments.
20. The concentrations of the microspheres with diameters of 0.60, 0.70, 0.80, 0.90, and 1.03 μm were 0.015, 0.010, 0.010, 0.005, and 0.005% solid, respectively.
21. H. C. Berg, *Random Walks in Biology* (Princeton Univ. Press, Princeton, NJ, 1993), p. 56.
22. The CV of particle diameter ϕ is defined as $\frac{\Delta\phi}{<\phi>} \times 100\%$, where $\Delta\phi$ is the standard deviation of ϕ and $<\phi>$ is the mean of ϕ. When used as a measure for resolution, CV is calculated according to
$$\frac{\frac{d\phi}{dx}\Delta x}{<\phi>} \times 100\%,$$
where x is the lateral position of the band, as a function of ϕ, and Δx is the measured standard deviation (half-width) of the band.
23. D. B. Sattelle, A. L. Obaid, B. M. Salzberg, *Biochem. Soc. Trans.* **19**, 501 (1991).
24. Duke Scientific Corp., Palo Alto, CA, personal communication.
25. K. Osoegawa *et al*., *Genome Res.* **10**, 116 (2000).
26. J. Sambrook, E. F. Fritsch, T. Maniatis, *Molecular Cloning: A Laboratory Manual* (Cold Spring Harbor Laboratory Press, Cold Spring Harbor, NY, ed. 2, 1989).
27. The DNA was isolated from *E. coli* strains RPCI 21 168-F5 and RPCI 22 49-E10. Plasmid preparations were digested with *Not*I and the digestion buffer exchanged with 1/2x TBE with the use of centrifugal filters (Microcon YM-100 from Amicon). We used 1/2x TBE as the electrophoresis buffer. Concentrations of 0.1% POP-6 and 10 mM dithiothreitol were added to suppress electroosmotic flow and photobleaching, respectively.
28. To calculate molecular-weight resolution, we assumed that the lateral position x of a band is a linear function of the radius of gyration of DNA, which is proportional to the square root of the molecular weight m, as described by the equation $x(m) = \sqrt{\frac{m}{k}} + x_0$, where x_0 and k are fitting constants. From Fig. 4A, we get $x_0 = -985$ μm and $k = 4.49 \times 10^{-5}$ kb/μm². By definition, we have $CV \equiv \frac{\Delta m}{m} = \frac{1}{m}\frac{dm}{dx}\Delta x = \frac{2k}{m}(x - x_0)\Delta x$, where Δx is the measured standard deviation (half-width) of the band.
29. Y. Kim, M. D. Morris, *Anal. Chem.* **67**, 784 (1995).
30. L. R. Huang *et al*., *Nature Biotechnol.* **20**, 1048 (2002).

31. Supported by grants from the Defense Advanced Research Projects Agency (MDA972-00-1-0031), NIH (HG01506), NSF Nanobiology Technology Center (BSCECS9876771), and the State of New Jersey (NJCST 99-100-082-2042-007). We thank K. Osoegawa and P. de Jong for supplying the bacterial artificial chromosome libraries; J. O. Tegenfeldt, P. Silberzan, S. Park, T. Duke, S. Weiss, D. Botstein, and P. M. Chaikin; and members of our laboratories for discussion. We acknowledge support from the Cornell University National Fabrication Center, where the deep silicon etching process of the device reported here was performed.

Supporting Online Material

www.sciencemag.org/cgi/content/full/304/5673/987/DC1

Fig. S1

10 December 2003; accepted 15 April 2004

Extra-Large–Pore Zeolites with Two-Dimensional Channels Formed by 14 and 12 Rings

Jean-Louis Paillaud,[1]* Bogdan Harbuzaru,[1] Joël Patarin,[1] Nicolas Bats[2]

Stable zeolites that have larger pore apertures and a three-dimensional pore topology are of interest because they could be used to adsorb larger molecules, particularly for application in oil refining. Several large-pore zeolitic materials with channels formed by openings of more than 12 rings are known, but all of them have a one-dimensional channel system that limits their use in catalysis. We report the synthesis and some characterizations of IM-12, a thermally stable germanium-containing zeolite that contains the first two-dimensional channel system with extra-large pores formed by 14- and 12-ring channels.

Because of their high thermal stability, new zeolites are of interest in petroleum refining, especially those with larger pores and systems of intersecting channels that could potentially process larger hydrocarbon molecules. Two approaches have led to larger pore systems. One is the use of fluoride ions in place of OH^- species (*1–3*), because the fluoride appears to act as a structure-directing agent (SDA) that plays a templating role (*4–6*). The other is the use of two sources of framework atoms. For example, the silicogermanates ITQ-12 (*7*), ITQ-17 (*8*), ITQ-21 (*9*), and ITQ-22 (*10*) present new topologies that include F^--containing double four-ring (D4R) cubic units in their structures (Scheme 1), thus confirming the template role of the F^- ion toward the formation of these D4R units. Interestingly, ITQ-17 (*11*) and ITQ-21 (*12*) can also be prepared in a fluoride-free medium, but at a slower crystallization rate. The formation of such porous structures is also related to the presence of Ge-O-Ge angles, which are smaller than the Si-O-Si angles that change the geometric constraints in the D4R units and thus stabilize the resulting structures (*13*). Theoretical calculations confirm this interpretation (*14*), together with the reported preferential occupation of the tetrahedral (T) sites of the D4R by Ge in the zeolites

[1]Laboratoire de Matériaux Minéraux, UMR-CNRS 7016, Ecole Nationale Supérieure de Chimie de Mulhouse, Université de Haute Alsace, 3 rue Alfred Werner, 68093 Mulhouse Cedex, France. [2]Institut Français du Pétrole, IFP-Lyon, Boîte Postale 3, 69390 Vernaison, France.

*To whom correspondence should be addressed. E-mail: jl.paillaud@uha.fr